AIRBORNE CO_2 COHERENT LIDAR MEASUREMENTS OF CLOUD OPACITIES OVER THE PACIFIC OCEAN

Robert T. Menzies
David M. Tratt
Jet Propulsion Laboratory
California Institute of Technology
Pasadena, CA 91109
U.S.A.
Tel: 1-818-354-3787

Pierre H. Flamant
CNRS Laboratoire de Meteorologie Dynamique
Ecole Polytechnique
91128 Palaiseau
FRANCE
Tel: 33-(1)-69.33.41.45

February 2, 1993

AIRBORNE CO_2 COHERENT LIDAR MEASUREMENTS OF CLOUD BACKSCATTER AND OPACITY OVER THE PACIFIC OCEAN

R.T. Menzies, D.M. Tratt, and P.H. Flamant

Abstract

The usc of an airborne CO_2 idar to obtain cloud backscatter and ext nction data at a thermal infrared wavelength is described. The extinction in this sı ectral region is proportional to the cloud liquid water content. The use of coherent detection results in high sensitivity and narrow FOV, the latter property greatly reducing multiple scattering effects. Backscatter measurements in absolute units are obtained through a hard target calibration methodology. Selected results are presented from data taken during flights over the Pacific ocean.

1. INTI{OD[JC11ON

An airborne CO_2 lidar was flown on the NASA DC-8 research aircraft during two extended missions over the Pacific ocean in 1989 and 1990. The objectives during these Pacific circumnavigations were to characterize aerosol backscatter levels at infrared wavelengths in relatively pristine regions of the troposphere, and to observe cloud properties in the thermal infrared and their effects on lidar signals. 'l'he lidar instrument responsivity was calibrated using a hard target methodology described in Kavaya and Menzies (1985) in order to provide quantitative aerosol and cloud volume backscatter coefficients and sea surface reflectance. The 9 μm wavelength of the airborne lidar instrument is of particular importance in support of the Earth-orbiting Laser Atmospheric Wind Sounder (1 .AWS, 1987) instrument design and performance studies.

In this paper we discuss the techniques for use of the coherent CO_2 lidar data taken in the nadir-viewing mode over the sea surface to derive various cloud optical properties at wavelengths in the thermal infrared, In addition to the obvious cloud top height determination these include the backscatter-to-extinction ratio, which is directly related to the integrated (attenuated) backscatter (Platt and Takashima, 1987), and for clouds of moderate optical thickness at the lidar wavelength, the optical depth at the lidar wavelength and the geometric thickness. From these measured quantities the liquid water content and mode radius can be derived for each case (Chylek, 1978; Platt and Takashima, 1987). The use of the sea surface reflectance signal permits calculation of the optical depth and expands the range of applicability. The use of coherent detection rather than direct detection results in increased sensitivity to the cloud backscatter as well as the attenuated sea surface backscatter below. It also mandates a significantly smaller field-of-view (FOV) than would normally be used in a direct detection lidar, resulting in negligible multiple scattering effects.

The typical flight altitudes for the GLOBE Pacific circumnavigation missions were in the 9-11 km region, although occasional cruise segments were at higher altitudes in order to be above cirrus. Thus in the nadir-viewing mode the lidar observations accessed low and mid-level clouds. A nadir-viewing CCD video camera provided simultaneous visible images during daylight hours, and a nadir-viewing radiometer with a therms] IR channel provided brightness temperatures along the flight track. Following descriptions of the instrument and measurement technique, two examples will be presented, one a case of a mid-level layer of altocumulus transitioning into altostratus as the aircraft proceeded along the flight track, anti the other a case of low-level stratocumulus.

2. INSTRUMENT DESCRIPTION

The JPL Airborne Backscatter Lidar (ABL) instrument consists of an injection-seeded TEA-CO_2 transmitter and a coherent receiver mounted on a stiff mechanical frame structure appropriate for the aircraft environment. The transmitter uses an unstable resonator cavity design which includes a grating for line selection. The output pulse energy is 1 Joule, and the prf during the GLOBE 1990 mission was usually set at 4 Hz. The receiver is a heterodyne receiver designed for range-gated detection of the atmospheric backscatter signal. A back-biased mercury-cadmium telluride p-n junction detector at 77 K was used as the photomixer. Separate cw CO_2 lasers were used as injection and local oscillators. The local oscillator (1.,0) resonator contained invar rod cavity length spacers, and the mechanical structure was modified to achieve adequate performance in the aircraft environment. During the GLOBE 1989 mission video detection was used following the amplification and bandpass filtering stages. A complex demodulator was fabricated and installed between the two GLOBE missions and used exclusively during the second mission in place of the video detection, Thus during the spring, 1990 mission two transient digitizers were used to sample the in-phase and quadrature lidar signals, each with 12-bit resolution and at a 10 MHz sampling rate. The data records were stored on a single pulse basis, to be pulse-averaged later if desired, thus providing maximum post-facto processing flexibility. The volume of recorded lidar data for a single flight ranged from 300-400 Mbytes. The instrument optics were pointed alternately in nadir or zenith modes, to collect vertical profile information throughout the troposphere.

"The instrument responsivity is calibrated in order to provide quantitative aerosol volume backscatter coefficients and reflectances from clouds and the sea surface. The calibration methodology which is used for the ABL instrument is based in large part on the techniques which are in use for the JPL ground-based lidar measurements of aerosol β profiles (Menzies, et al., 1984; Kavaya and Menzies, 1985; Ancellet et al., 1988). A flame-sprayed aluminum hard target approximately 2 meter square is deployed at a range of 1-2 km from the lidar after installation in the aircraft, and the lidar responsivity is calibrated from the multiple-shot-averaged signal return. The atmospheric attenuation coefficient along the path is determined by observing the aerosol backscatter signal intensity vs. range over nearly horizontal paths along the same azimuth. Separate measurements of humidity and temperature are made, and the molecular contribution to the tots] attenuation is calculated based on these measurements. This technique for

determining the boundary layer attenuation assumes the existence of enough horizontal homogeneity to use the slope method. The modeling of the atmospheric attenuation vs. altitude when in the flight mode presently includes only the molecular contribution above the boundary layer, and standard models are ordinarily used for profiles of temperature, CO_2, and water vapor. (Further discussion of the atmospheric attenuation effects on retrievals of quantitative backscatter coefficients is contained in the next section.)

The overall calibration of lidar aerosol backscatter data requires an understanding of several factors, some of which can be described as subtle and complex (as noted in e.g., Kavaya and Menzies, 1985). There are also several practical considerations which are unique to the airborne configuration. These are continuing to be assessed in order to minimize errors associated with calibration of the instrument.

3. MEASUREMENT TECHNIQUE

a. *Determination of Cloud Optical Properties from the Lidar Measurement*

When the lidar is probing a single cloud layer from above, the backscatter coefficient as a function of depth is obtained, until the point is reached at which the return signal falls below the level of sensitivity of the lidar. For clouds of moderate optical thickness, the lidar signal from the surface below can be observed. Platt and Takashima (1987) show that for an optically thick $\tau_{OL} \gg 1$, whether viewing from above or below, the attenuated cloud volume backscatter coefficient, $\beta'_c(\pi, z)$, (defined as $\beta = B/4\pi$, where B is the isotropic backscatter coefficient used in Platt and Takashima (1987)), which is the quantity measured by the lidar, is related to the backscatter-to-extinction ratio. The attenuated cloud volume backscatter coefficient can be defined as

$$\beta'_c(\pi,z) = \beta_c(\pi,z) \exp\left[-2\int_{z_T}^{z} \eta(z') \sigma_c(z')dz \right] \qquad (1)$$

where $\beta_{c(\pi,z)}$ is the unattenuated volume backscatter coefficient, $\sigma_{c(z)}$ is the volume extinction coefficient, $\eta(z)$ is a multiple scattering factor, and z_t is the cloud top. (It is assumed that the lidar is above the cloud, sounding vertically downward, as in Platt, et al., (1989).) Platt and Takashima point out that if the backscatter to extinction ratio,

$$k = \beta_c(\pi,z) / \sigma_c(z) \qquad (2)$$

and the multiple scattering factor, T-I(z), arc assumed constant through the probed region of the cloud, then the integral of $\beta'_c(\pi,z)$, which is the integrated attenuated backscatter, $\gamma'(\pi)$, can bc expressed as

$$\gamma'(\pi) = (k/2\eta)\{1 - \exp[-2\eta\delta_c]\} \quad (3)$$

i.e., the integrated attenuated backscatter, which is a lidar observable, can be expressed is terms of the backscatter-to-extinction ratio, the multiple scattering factor, and the cloud optical depth, δ_c, at the lidar wavelength. The multiple scattering effects add complication and error.

h. *Multiple Scattering Considerations*

The use of a coherent lidar such as the ABL instrument renders multiple scattering effects insignificant and simplifies the relationships. In the airborne lidar geometry, the multiple scattering will be most apparent when the backscattered signal on its return to the lidar receiver has been forward scattered one or more times at very small angles and can contribute to the signal. Multiple backscattering is less probable, (The asymmetry factor $<\cos\theta>$ for water spheres ranges from approximately 0.1 to 0.9 for radii between l-pm and 10-μm, respectively, for $\lambda = 9.25$ μm (Irvine and Pollack, 1968), and the scattering efficiencies increase with radius in this range.) The multiple scattering contribution depends on the lidar field-of view, the cloud optical depth, ant] the single scattering albedos and the phase functions of the particles. The very narrow FOV of the coherent lidar, which must operate in a diffraction-limited mode, in addition to the relatively long lidar wavelength, result in higher order scattering effects being negligible. For the case of the ABL instrument, the transmitter full angle divergence in the far field is 200 μrad.

The scattering contributions to the reduction of the measured extinction can be considered in two categories. The first is a forward-scattering for which the scattered radiation falls within the FOV of the lidar receiver. Forward-scattering corrections for a mid-visible wavelength were calculated by Deepak and Box (1978) for a number of polydispersions of the modified Gamma type, assuming spherical particles. Bohren and Koh (1985) calculated forward-scattering extinction corrections for certain classes of non-spherical particles. Using the notation of Bohren and Koh (1985), the measured extinction cross section C'_{ext} of the ensemble of cloud particles is reduced from the actual extinction cross section by an amount depending on how much light is scattered

into the lidar receiver acceptance angle

$$C'_{ext} = C_{ext} - \int_{\Omega_{acc}} \frac{dC_{sca}}{d\Omega}\, d\Omega \qquad (4)$$

For example, we have calculated the forward-scattering extinction correction for a Deirmendjian Cl model size distribution:

$$n(r) = ar^6 \exp(-3r/2) \qquad (5)$$

where n(r) is the number of particles per unit interval of radius (μm) and per unit volume, and the integral over, eqn. (5) is set equal to N = 100 cm^{-3}. (The mode radius for the Cl size distribution is 4 μm.) Using a Mie scattering code, with complex refractive index values for water at the 9.25 μm wavelength from Hale and Querry (1973), the value of the first term of eqn. (4) is C_{ext} = 143,4 μm^2, and the integrand of the second term of eqn. (4) has been calculated to be $dC_{sca}/d\Omega$ = 216 $\mu m^2\, sr^{-1}$. The lidar acceptance angle is 1.8 x 10^{-8} sr. Thus the correction term is equal to 3.9 x 10^{-6} μm^2, which is insignificant. The second category is multiple scattering when the radiation has experienced more than one forward scattering process with a final propagation direction within the receiver FOV. Using a propagation model described by Bissonnette (1988), which is an approximation relevant to the propagation of narrow beams and small observation fields-of-view, calculations for a few representative scattering particle radii up to 20 μm indicate that this effect contributes less than a part in 10^5 to the signal for the range of cloud types and optical depths considered.

c. Use of Sea-Surface Reflectance Signal for Direct Cloud Opacity Measurement

A significant advantage of the airborne lidar flying over open water is the additional direct cloud opacity measurement which is possible in addition to the backscatter and integrated backscatter. As stated earlier, the integrated attenuated backscatter can be related directly to k, the backscatter-to-extinction ratio, as in Eqn. (3), if the cloud optical depth is known, or if the cloud optical depth is large enough to neglect the second term. It has been determined from analysis of ABL data taken in a nadir-viewing mode over the Pacific that the sea surface reflectance signal is relatively steady over flight track lengths which are long compared with spatial scales of variability of many cloud types. This permits the "clear atmosphere" sea surface signal to be used

as a reference intensity in the calculation of cloud opacity as clouds are encountered along the flight track. For most cases when viewing clouds of moderate optical thickness, such that the sea surface signal is above the lidar receiver noise level, porous regions in the cloud cover occur often enough to permit a "recalibration" of the sea surface reflectance signal sufficiently often. Most of the lidar data taken during the GLOBE Pacific Missions were from altitudes near 10 km. From this altitude the typical maximum observable (single pass) optical depth ranges from 4-5, depending on the magnitude of the sea surface reflectance signal and the pulse averaging.

d. Atmospheric Extinction Effects as Potential Sources of Error

The effects of atmospheric extinction on the cloud backscatter and opacity retrieval accuracy are linked to the measurement or modeling of temperature and water vapor mixing ratio profiles. Molecular absorption losses at the lidar wavelength are due to the $C0_2$ hot band transition which is the laser line and the water vapor continuum. Small tropospheric ozone losses occur also, amounting typically to 4-5% (2-way) absorption through the lower 10 km of the troposphere at mid-latitudes. Aerosol extinction at the lidar wavelength is typically no more than $0.1 km^{-1}$ even in a low visibility marine boundary layer. The brightest elevated aerosol layers observed over the Pacific were due to dust transport from the Asian continent. The observed backscatter coefficients from these layers reached levels as high as $10^{-7} m^{-1} sr^{-1}$ in a few cases. The extinction-to-backscatter ratio for dust at 10 μm is about 30 sr (Carlson and Benjamin, 1980), with somewhat higher values at 9.25 μm due to the presence of refractive index resonances; consequently, the extinction levels for these layers were below 0.01 km^{-1}.

The molecular absorption effects can be taken into account quite effectively with modeling and use of available global analysis data products. The temperature and molecular extinction profiles for the AFGL Tropical and Midlatitude Summer models (McClatchey, et al., 1972) are presented in Figures 1 and 2, the extinction profiles corresponding to the lidar wavelength. (The models representing colder troposphere produce reduced molecular extinction.) Molecular extinction is significant only in the lower troposphere, where the temperature difference between the two models is 3-4 K. For the CO_2 absorption of the 9R(24) laser line, a 1 % increase in temperature near 300 K results in an increase of about 6% in the absorption coefficient. Previous analyses of errors due to incorrect atmospheric modeling (Kavaya and Menzies, 1985) lead to the conclusion that, e.g., if the troposphere were actually Tropical and the lidar retrieval algorithm assumed Midlatitude Summer the integrated error in determination of cloud

backscatter coefficient could reach 25% for observation of low clouds (marine stratocumulus) from a nominal 10-km altitude. The error would be less for mid-level clouds due to the correspondingly shorter ranges from the lidar. The available global analysis data products can be used to characterize the tropospheric temperature and humidity profiles with uncertainties less than the MLS and TRO Model differences, implying that the worst case errors in backscatter retrievals can be maintained well below the 25% level. Use of on-board IR radiometer data can further reduce the uncertainties in atmospheric transmittance.

Considering boundary layer extinction effects, it is the variability of the boundary layer extinction which is a potential source of error in measurement of cloud opacity using the sea surface reflectance signal, rather than the lack of knowledge of the absolute transmittance through it. A homogeneous boundary layer (over the relevant horizontal spatial scales) would not affect the accuracy of the cloud backscatter and opacity measurements because the cloud layers are between the lidar and the boundary layer. The boundary layer height and the aerosol backscatter coefficients within the boundary layer can be observed when clear sky paths to the sea surface are available. It is recognized that the characteristics of the boundary layer under cloud cover will differ from those under a cloud-free sky. Thus it is advisable to obtain a reference measurement of the sea surface reflectance in a clear region in the vicinity of the cloud field. For the case of scattered or broken cloud cover, this is feasible. The boundary layer extinction will reduce the lidar SNR for observation of the sea surface reflectance signal; however, this is not a severe limitation. The presence of a boundary layer even with relatively high molecular and/or aerosol extinction losses would reduce the maximum observable cloud optical depth by an amount no greater than 0.5.

e. Determination of Cloud Liquid Water Content and Mode Radius

It has been pointed out by several authors (e.g., Platt, 1976; Chylek, 1978; Pinnick, et al., 1979; Chylek, et al., 1992) that the cloud extinction coefficient measured in the 8-12 μm wavelength region is approximately a linear function of liquid water content, W (g m^{-3}), with various levels of accuracy depending on the wavelength and the cloud droplet size distribution. Chylek, et al. (1992) point out that higher order terms in a polynomial expansion are necessary in order to minimize errors for a wide variety of cloud types. However, one can conclude from their analysis that for the cloud types of low to moderate values of W, which correspond to the layers of small to moderate optical thickness considered here, the accuracy of the linear approximation at the 9.25

μm wavelength is very good, with typical errors less than 5%.

At wavelengths in the thermal infrared the value of the backscatter-to-extinction ratio *k* depends in a rather systematic way on the mode radius, as pointed out by Platt and Takashima (1987). On the contrary, the value of this parameter when using visible or near infrared wavelengths is nearly independent of the cloud size distribution, being approximately 0.05 for a variety of water cloud types (Pinnick, et al., 1983), The relationship between the value of the backscatter-to-extinction ratio and the mode radius is not as definitive as is the linear relationship between the extinction coefficient and the cloud liquid water content. Nonetheless the dependence of *k* on mode radius for the ABL wavelength, renders it possible to obtain at least an approximate indication of the most probable droplet sizes.

4. EXPERIMENTAL DATA

In this section we present two examples using ABL data taken during the GLOBE Pacific circumnavigation during the spring of 1990. The lidar data taken during this series of flights has been processed using false color display plotting. These plots indicate vertical profiles of volume backscatter coefficient in calibrated absolute units, with vertical resolution of approximately 150 m and a standard horizontal resolution of about 500 m, corresponding to a 10-shot average per vertical strip. This "quick look" data display format permits the recognition of both vertical layering and the extent of horizontal homogeneity at a given altitude. The typical color bar scale ranges over 5 orders of magnitude in backscatter coefficient. For studies of the cloud properties the data are available on a single-shot basis, corresponding to horizontal averaging over a lidar footprint of typically 1-2.5 m, depending on the range to the cloud. The fundamental (non-smoothed) vertical resolution is approximately 100 m, due to the pulse temporal shape, although the leading edge (cloud top height) can be determined with higher resolution due to the short rise time of the pulse shape. The digital sampling frequency of the lidar signal was 10 MHz.

Video cameras mounted on the DC-8 aircraft permitted viewing of visible images of the clouds below the aircraft during daylight hours. A nadir-directed Barnes PRT-5 radiometer produced measurements of the upwelling radiance in the thermal IR window region along the flight track, with a resolution of 2°,

"l'he first example is an observation of a mid-level cloud layer near the end of a transit flight between Darwin, Australia and Yokota AFB (near Tokyo), Japan. The

lidar data are shown in Figure 3, along with the corresponding calculated cloud optical thickness along the same portion of the flight track. The aircraft altitude is approximately 11 km (37,000 ft) until a slow descent begins to occur near the 50 krn point along the flight track. The thin cloud layer is observable between 4 and 5 km altitude. The band across the bottom is the (attenuated) sea surface reflectance signal. (When the lidar backscatter signal falls below the 2-u receiver noise threshold, the corresponding region is white. In regions where the backscatter is consistently below the lidar sensitivity threshold, the pattern is one of occasional randomly positioned colored pixels appearing on a white background, due to the occasional speckle spikes which rise above the threshold level.) The horizontal resolution for this example is approximately 500 m. The maximum optical thickness in this case (a round-trip path optical thickness of approximately 8) is due to the instrumental SNR limitation, the sea surface reflectance signal dropping below the noise level for greater optical thicknesses, According to the videotape view of the mid-level cloud layer seen in this example, the morphology changes from altocumulus translucidus (semi-transparent) to altocumulus cumulogenitus and then altocumulus floccus, until the halfway point is reached (near 40 km), where it changes to a veil of altostratus, becoming thin and wispy (translucidus) in the 53-65 km region of the flight track. The lidar observations of opacity variability at 9.25 μm wavelength are very consistent with the qualitative visual indications. In Figure 4 the corresponding IR radiometer derived brightness temperature is plotted along with the lidar derived cloud optical thickness. Even though the cross-track resolution of the radiometer (200 r-n) is much broader than that of the lidar, the features correlate very well. The region of large optical thickness indicates a cloud top temperature of 0° C, and the region of high transparency indicates a surface temperature near 20° C.

The integrated attenuated backscatter for this example is plotted in Figure 5. During the altocumulus portion the integrated backscatter oscillates about a rather stable value (average value of 1.75 x $10^{-4} sr^{-1}$). The double-pass optical depth, $2\delta_c$, ranges from 4 to greater than 8 during this period, leading to values of σ_c ranging from *1-2 x* $10^{-2} m^{-1}$ and corresponding values of liquid water content W = 5-lox 10^{-2} g m^{-3}. The average value of the backscatter-to-extinction ratio during the altostratus region (excluding the porous regions between 52-60 km and 64-67 km along the track) is much higher than that of the earlier altocumulus region, approximately 2.5 times higher in the 46-52 km region and an order of magnitude higher in the 60-64 km region. This is consistent with previous conclusions that the backscatter-to-extinction ratio at thermal IR wavelengths is highly dependent on cloud droplet size distribution, varying by more than an order of

magnitude (Pinnick et al., 1983). The calculated liquid water content W in the regions of altostratus which are not visibly porous ranges from 1.2-3 x 10^{-2} g m^{-3}.

The higher values of backscatter-to-extinction ratio observed over the optically thin altostratus portions of this example imply smaller mode radii, since *k* decreases with increasing mode radius (r_c). Using the curve fit from Platt and Takashima (1987), mode radii ranging from 2 μm for the thin altostratus to over 10 μm for the altocumulus are estimated.

The second example is an observation of a transition zone between clear atmosphere and solid stratocumulus at the top of the marine boundary layer. In Figure 6 the clouds are scattered and of low to moderate optical thickness. The aircraft altitude is just over 8 km (27,000 ft), and the horizontal resolution in this example is approximately 100 m, corresponding to a 2-shot average for each resolution element. The atmosphere above the cloud level is quite clean, with no well-defined regions of atmospheric backscatter above the noise level (for 2-shot averaging) until the clouds and boundary layer aerosol below are reached. In the regions of large optical depth, the derived liquid water content W ≥ 0.1 g m^{-3}, however there are several distinct cloud features for which the optical thickness is much smaller and W ranges from 2-3 x 10^{-2} g m^{-3}. The values of the integrated backscatter and corresponding values of *k*, as shown in Figure 7, are much higher than observed for the altocumulus in the first example. 'l'his underscores the fact that the backscatter-to-extinction ratio is very sensitive to the cloud microphysical characteristics. One can conclude that the mode radii for these low-level stratocumulus are much smaller than for the altocumulus, being near 2 μm.

The derived cloud parameters from these two examples are segregated into four cloud type categories (the altostratus-1 referring to the 47-53 km region of the flight track, and the altostratus-2 referring to the translucidus in the 60-64 km region) and summarized in Table I.

5. CONCLUSIONS

We have described a method for obtaining cloud optical properties and derived liquid water content and mode radius, using airborne CO_2 backscatter lidar with coherent detection. The basic relationships between the backscatter, integrated backscatter, and extinction data obtained from the lidar and the cloud properties have been described previously by Platt and Takashima (1987). The use of airborne coherent lidar, as described here, permits in many cases the additional measurements of the cloud

opacity and geometric thickness at a thermal infrared wavelength, which are difficult, if not impossible, to obtain using ground-based lidars or radiometers. Multiple scattering effects for the JPL airborne backscatter lidar, which is representative of coherent IR lidars, are not a significant factor, The potential errors in computed cloud backscatter and extinction due to atmospheric extinction along the path to the cloud or to the sea surface can be reduced to levels which are generally satisfactory through the use of appropriate models or available global analysis data products. Measurement of backscatter levels to an accuracy much better than ± 25 % would require ancillary sensor data; however, uncertainties associated with other lidar calibration factors make it difficult to achieve much better accuracy levels in any event.

Two examples of data obtained using the JPL airborne backscatter lidar during a GLOBE Pacific circumnavigation mission have been presented. These are examples of stratocumulus, altocumulus, and altostratus of low to moderate optical depths and geometric thicknesses of 150-300 m. "l'he derived cloud properties are generally consistent with those derived from models of these cloud types. The strong lidar backscatter observed from the thin altostratus of very low optical thickness is evidence of the sensitivity of the lidar observations of thin clouds, even at a 9.25 μm wavelength, for which the backscatter-to-extinction ratio is generally at least an order of magnitude below that at visible and near infrared wavelengths.

The use of the sea surface reflectance signal to measure cloud opacities as described in this paper is applicable for cloud optical depths as large as 4-4.5 for data obtained from the GLOBE Pacific circumnavigation missions. The emphasis of these missions was to survey the aerosol and cloud backscatter levels throughout the depth of the troposphere. A more optimized approach to the cloud measurements described here would entail a flight altitude much closer to the cloud top level, and greater smapling density using a higher lidar prf and/or a slower aircraft cruise speed, The higher signal-to-noise levels resulting from these optimization would permit measurements for optical depths in the range of 6-8 for low and mid-level clouds.

Acknowledgements

The authors would like to acknowledge the contributions of A. Brothers, S. Dermenjian, and C, Esproles during the ABL flights, and helpful discussions with R.A. West and with J. Spinhirne and W. Wiscombe of NASA Goddard Space Flight Center. This work was carried out by the Jet Propulsion Laboratory, California Institute of q'ethnology, under contract with the National Aeronautics and Space Administration.

REFERENCES

Ancellet, G. M., R.T. Menzies, and D.M. Tratt, "Atmospheric backscatter vertical profiles at 9.2 and 10.6 μm: a comparative study", Appl. Opt.. 27, 4907-4912, 1988.

Bissonnette, L. R., "Multiscattering Model for Propagation of Narrow Light Beams in Aerosol Media", Appl. Opt,. 27, 2478-2484, 1988.

Bohren, C. F., and G. Koh, "Forward-scattering Corrected Extinction by Nonspherical Particles", Appl. Opt.. 24, 1023-1029, 1985.

Carlson, T. N., and S.G. Benjamin, "Radiative Heating Rates for Saharan Dust", J. Atmos. Sci., 37, 193-213, 1980.

Chýlek, P., "Extinction and Liquid Water content of Fogs and Clouds", J. Atmos. Sci., 35, 296-300, 1978.

Chýlek, P, P. Damiano, D. Ngo, and R.G. Pinnick, "Polynomial Approximation of the Optical Properties of Water clouds in the 8-12 μm Spectral Region", J. Appl. Meteor.. 31, 1210-1218, 1992.

Deepak, A., and M.A. Box, "Forwardscattering Corrections for Optical Extinction Measurements in Aerosol Media, 2: Polydispersions", Appl. Opt., 17, 3169-3176, 1978.

Hale, G. M., and M.R. Querry, "Optical Constants of Water in the 200 nrn to 20 μm Wavelength Region, APp1. Opt., 12, 555-563, 1973.

Irvine, W.M. and J.B. Pollack, "Infrared Optical Properties of Water and Ice Spheres", Icarus, 8, 324-360, 1968.

Kavaya, M. J., and R.T. Menzies, "Lidar Aerosol Backscatter Measurements: Systematic, Modeling, and Calibration Error Considerations", Appl. Opt., 24, 3444-3453 (198 S).

LAWS (Laser Atmospheric Wind Sounder) Instrument Panel Report, Earth Observing System, volume IIg (NASA, Washington, D. C., 1987).

McClatchey, R. A., Fenn, R. W., Selby, J. E. A., Volz, F. E., and Garing, J. S., Optical Properties of the Atmosphere (Third Edition), AFCRI..-72-0497, AD 753-075 (1972).

Menzies, R. T., M.J. Kavaya, P.H. Flamant, and D.A. Haner, "Atmospheric aerosol backscatter measurements using a tunable coherent CO_2 lidar, Appl. Opt. 23, 2510-2516, 1984.

Menzies, R. T., G.M. Ancellet, D.M. Tratt, M.G. Wurtele, J.C. Wright, and W. Pi, "Altitude and seasonal characteristics of aerosol backscatter at thermal IR wavelengths using lidar observations from coastal California", J. Geophys. Res., 94, 9897-9908, 1989.

Pinnick, R. G., S.G. Jennings, P. Chýlek, and H.J. Auvermann, "Verification of a Linear Relationship between IR Extinction, Absorption, and Liquid Water Content of Fogs", J. Atmos. Sci., 36, 1577-1586, 1979.

Pinnick, R. G., S.G. Jennings, P. Chýlek, C. Ham, and W.T. Grandy, Jr., "Backscatter and Extinction in Water Clouds", J. Geophys. Res., 88, 6787-6796, 1983.

Platt, C. M. R., "Infrared Absorption and Liquid Water Content in Stratocumulus Clouds", Quart. J. Roy. Meteor. Sot., 102, 553-561, 1976.

Platt, C. M. R., and T. Takashima, "Retrieval of Water Cloud Properties from Carbon Dioxide Lidar Soundings", Appl. Opt., 26, 1257-1263, 1987.

Platt, C. M. R., J.D. Spinhirne, and W.D. Hart, "Optical and Microphysical Properties of a Cold Cirrus Cloud: Evidence for Regions of Small Ice Particles", J. Geophys. Res., 94, 11,151-11,164, 1989.

Table I. Parameters for Cloud Examples Observed by Airborne Lidar

Cloud type	k (sr^{-1})	W ($g\ m^{-3}$)	r_c (μm)
Altocumulus	3.5×10^{-4}	$5\text{-}1o \times 10^{-2}$	10
Altostratus-1	9×10^{-4}	3×10^{-2}	6
Altostratus-2	3.5×10^{-3}	1.2×10^{-2}	3
Stratocumulus	$4\text{-}6 \times 10^{-3}$	2-8 X 10-2	2

FIGURE CAPTIONS

Figure 1. Ternperatur eprofiles in the troposphere for two models (McClatchey, et al., 1972) commonly used for computations of atmospheric molecular absorption at the lidar wavelength.

Figure 2. Molecular (CO_2, H_2O) absorption profiles atthe 9.25 μm lidar wavelength for the same models.

Figure 3. Time series showing: (top) distinct mid-level cloud layer at 4.5 km altitude, with uniform aerosol layers above, and (bottom) corresponding variation of inferred cloud optical thickness along the flight track.

Figure 4. Simultaneous upwelling thermal IR radiance (above) and atmospheric optical thickness (below) for the same flight track as in Figure 3 (Transit Darwin, Australia to Tokyo, Japan, May 31, 1990).

Figure 5, Integrated backscatter through the mid-level cloud layer for the same flight track,

Figure 6. Time series showing (top) scattered cumulus cells in a transition zone between clear air and stratocumulus, and (bottom) corresponding variation of inferred optical thickness due to the clouds along the flight track.

Figure 7. Integrated backscatter along the same flight track as in Figure 6 (Honolulu, HI to Mountain View, CA, June 5, 1990).

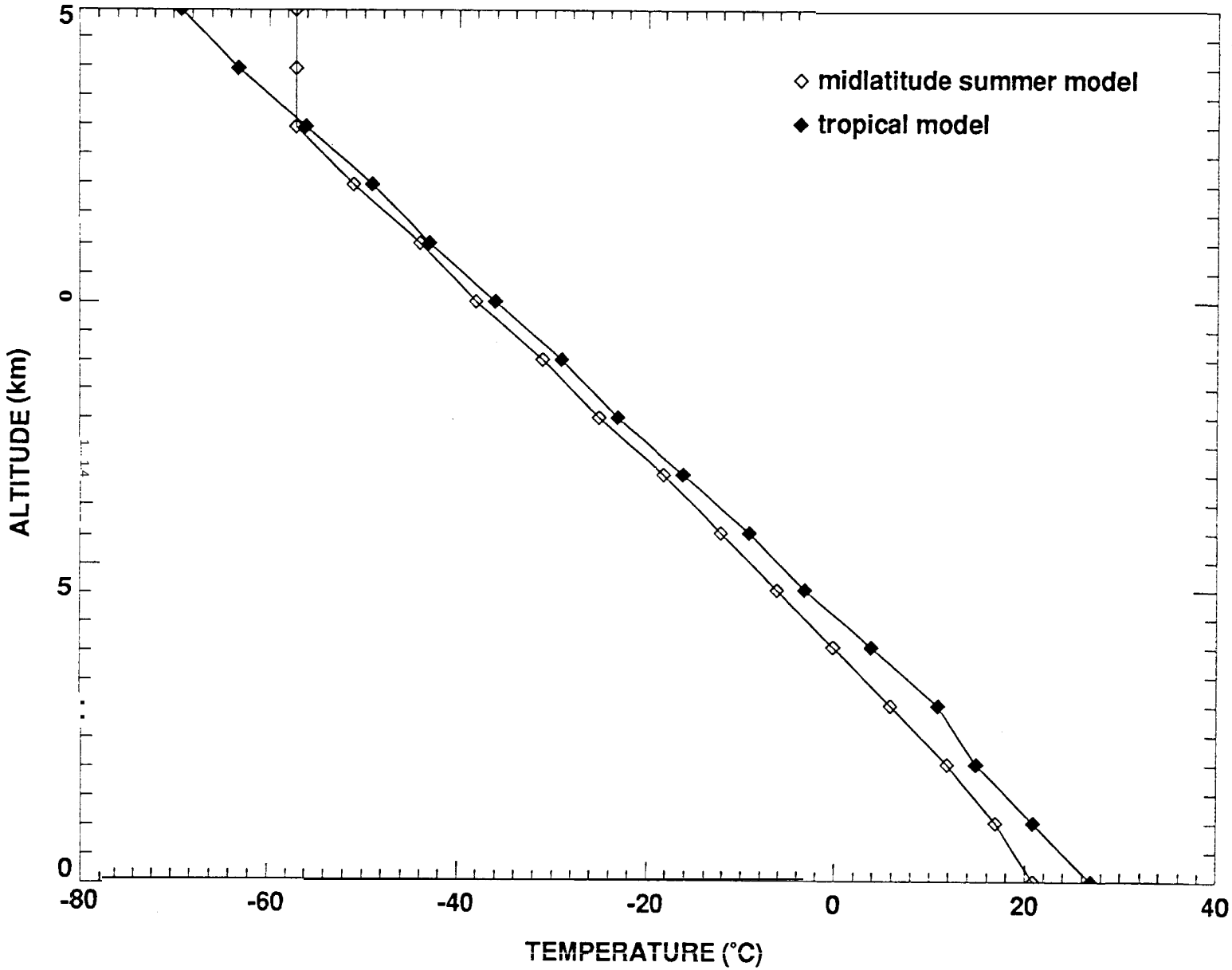
midlatitude summer model
tropical model
ALTITUDE (km)
TEMPERATURE (°C)
5
0
5
0
-80
-60
-40
-20
0
20
40

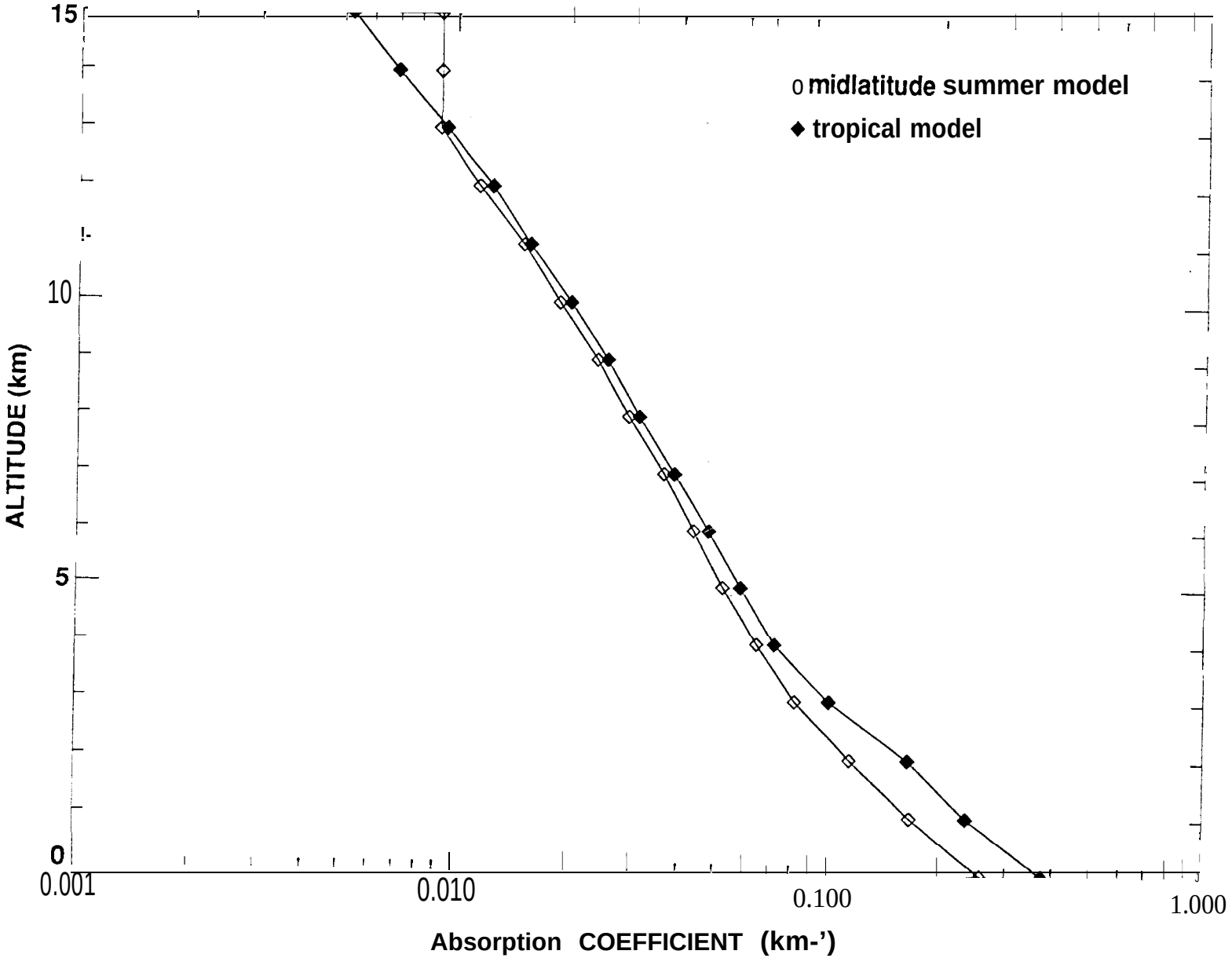
15
10
5
0
ALTITUDE (km)
o midlatitude summer model
◆ tropical model
0.001
0.010
0.100
1.000
Absorption COEFFICIENT (km-')

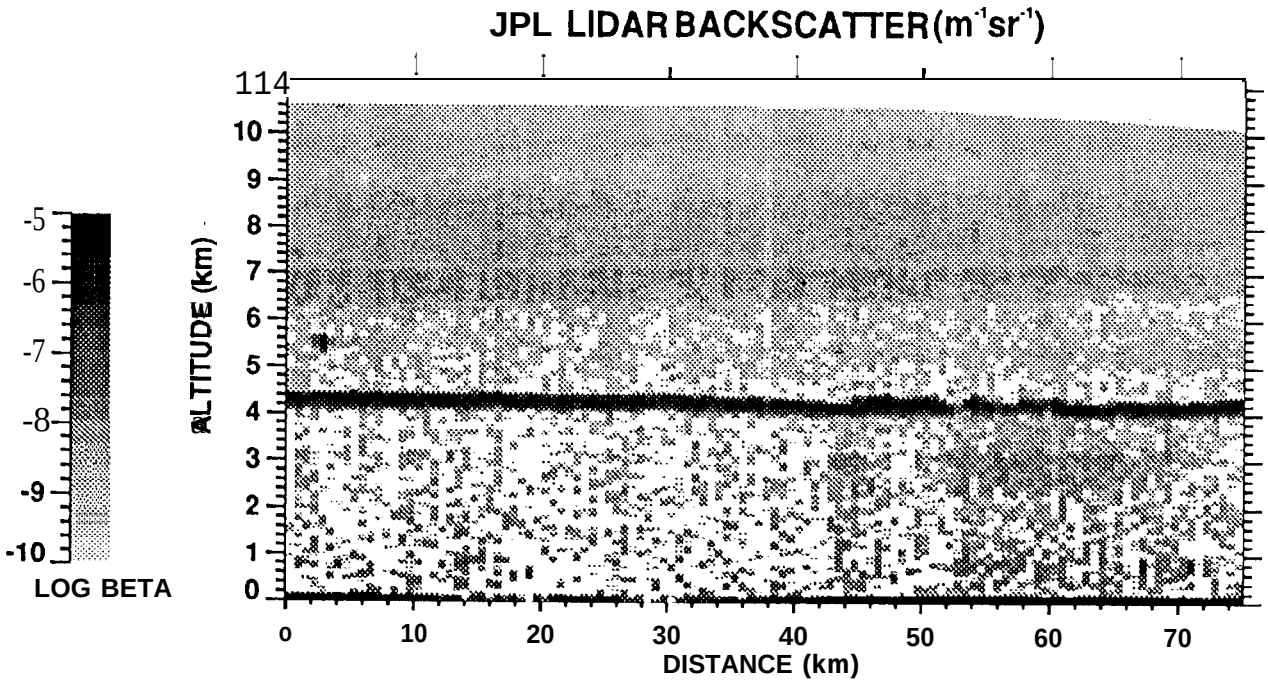

GLOBE 90 FLT 90-02-12 DAY: 151 MAY 31, 1990
TRANSIT DARWIN, AUSTRALIA TO YOKOTA AFB, JAPAN
FILE 80 START TIME: 06:54:03 END TIME: 06:59:31 UTC
ALTITUDE: FL370

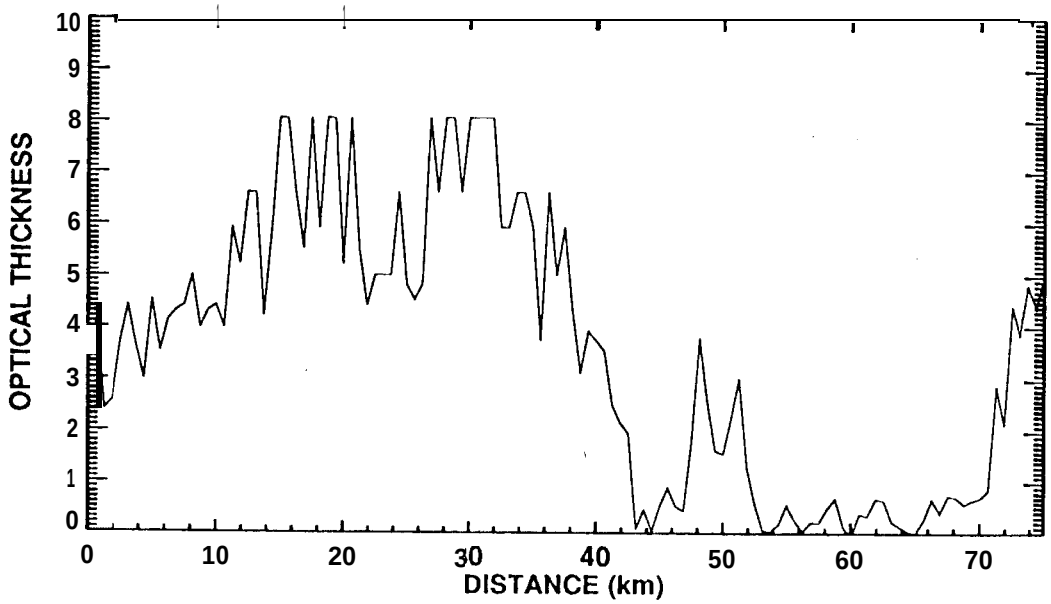

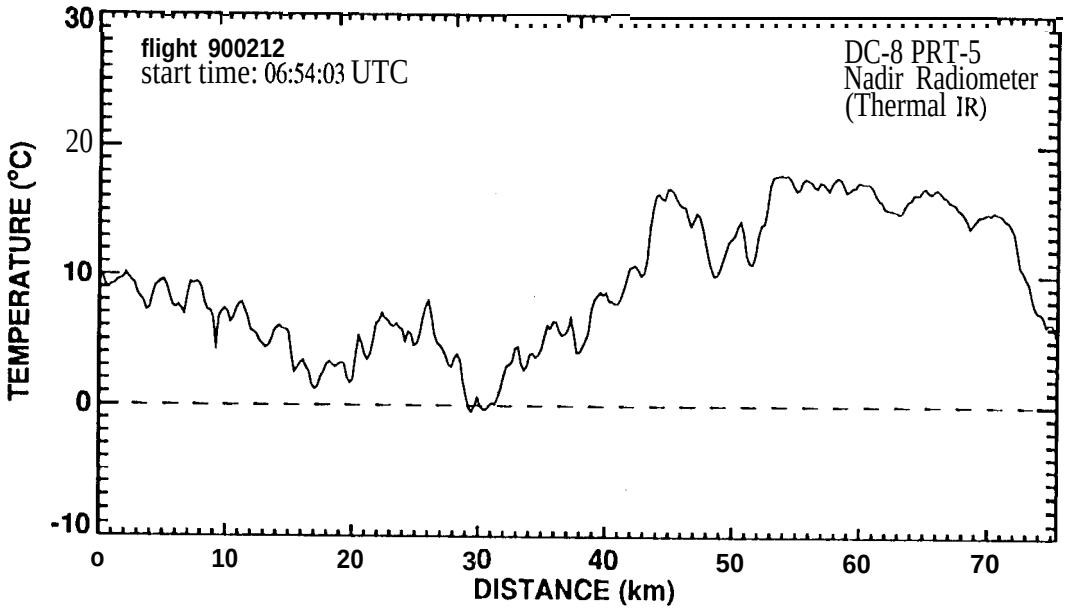
flight 900212
start time: 06:54:03 UTC
DC-8 PRT-5
Nadir Radiometer
(Thermal IR)
TEMPERATURE (°C)
30
20
10
0
-10
0
10
20
30
40
50
60
70
DISTANCE (km)

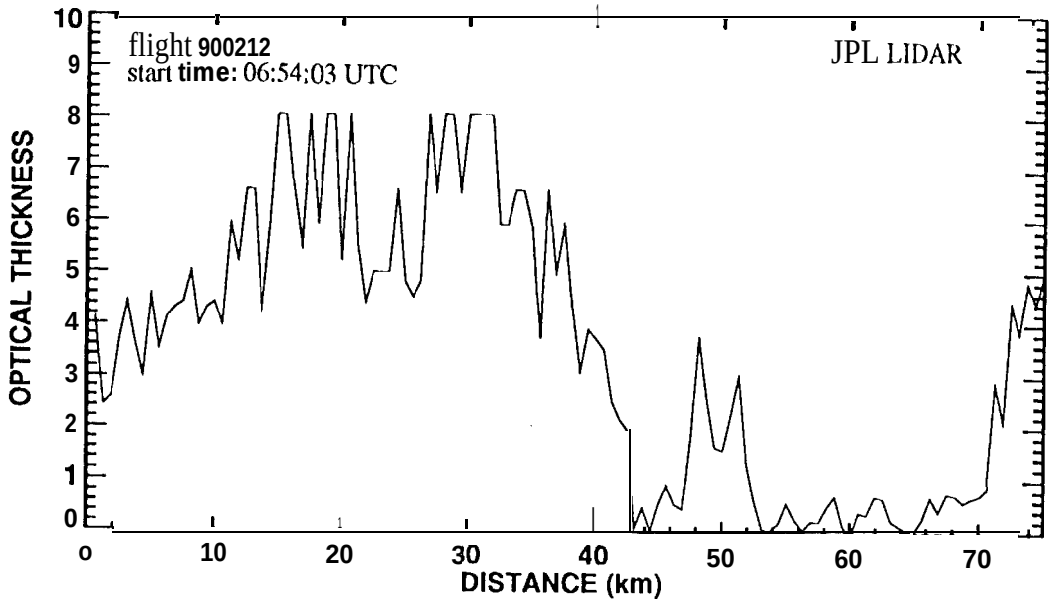
flight 900212
start time: 06:54:03 UTC
JPL LIDAR
OPTICAL THICKNESS
10
9
8
7
6
5
4
3
2
1
0
0
10
20
30
40
50
60
70
DISTANCE (km)

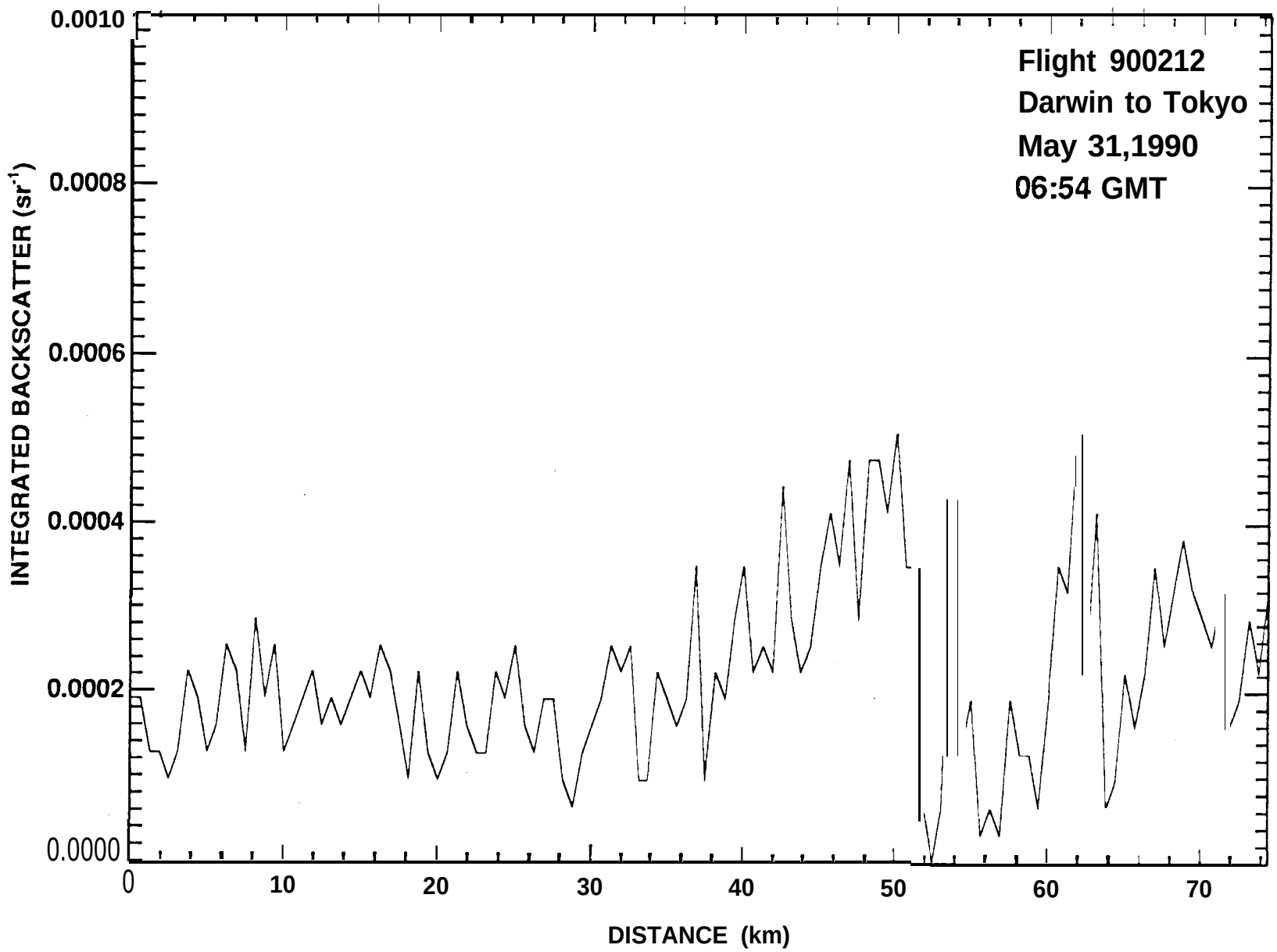
Flight 900212
Darwin to Tokyo
May 31,1990
06:54 GMT
INTEGRATED BACKSCATTER (sr-1)
0.0010
0.0008
0.0006
0.0004
0.0002
0.0000
0
10
20
30
40
50
60
70
DISTANCE (km)

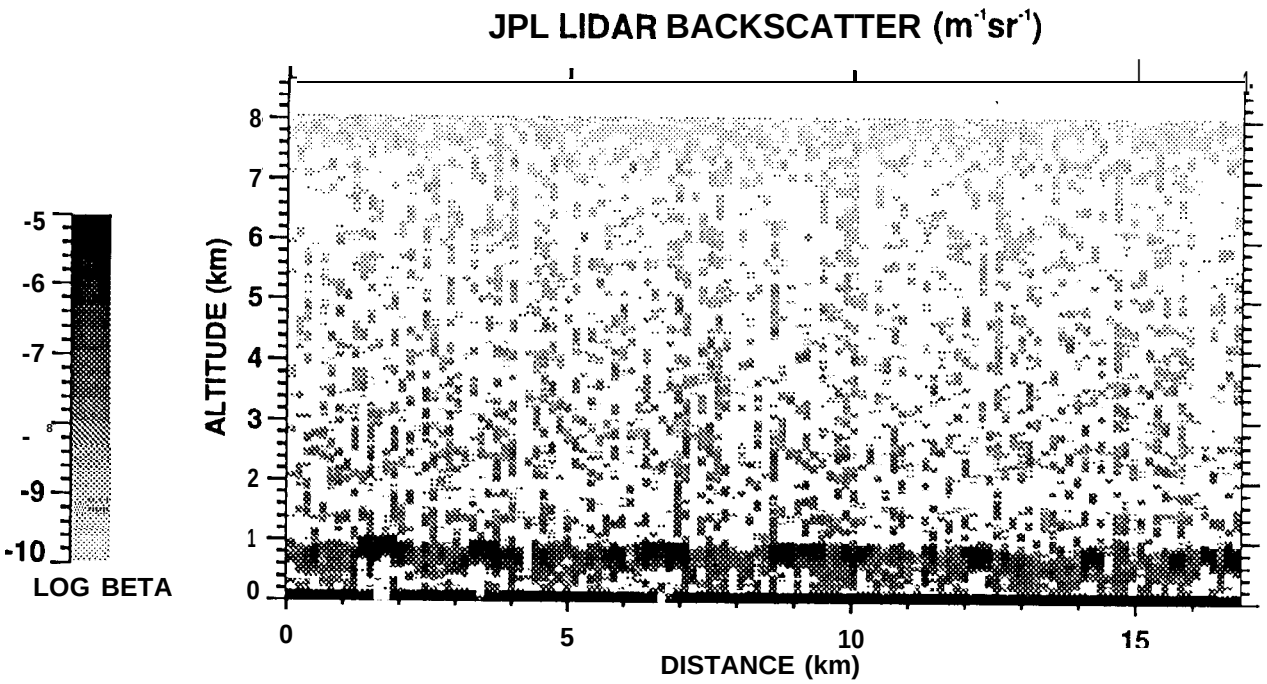

GLOBE90 FLT 90-02-15 DAY: 156 JUNE 5,1990
TRANSIT HICKAM AFB, HI TO MOFFETT FIELD NAS, CA
FILE 51 START TIME: 20:58 END TIME: 20:59 UTC
ALTITUDE: FL270

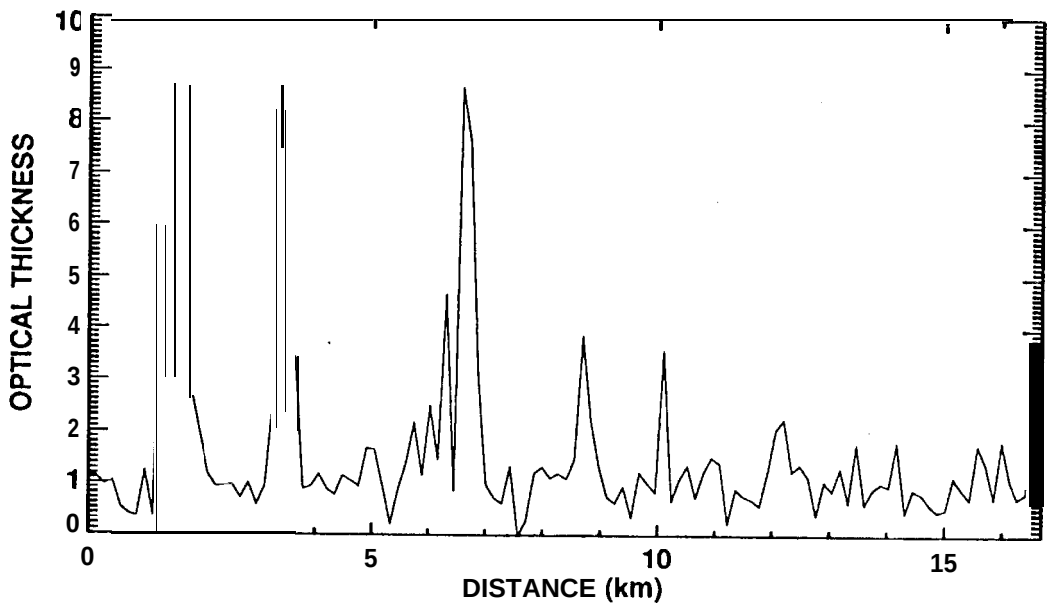

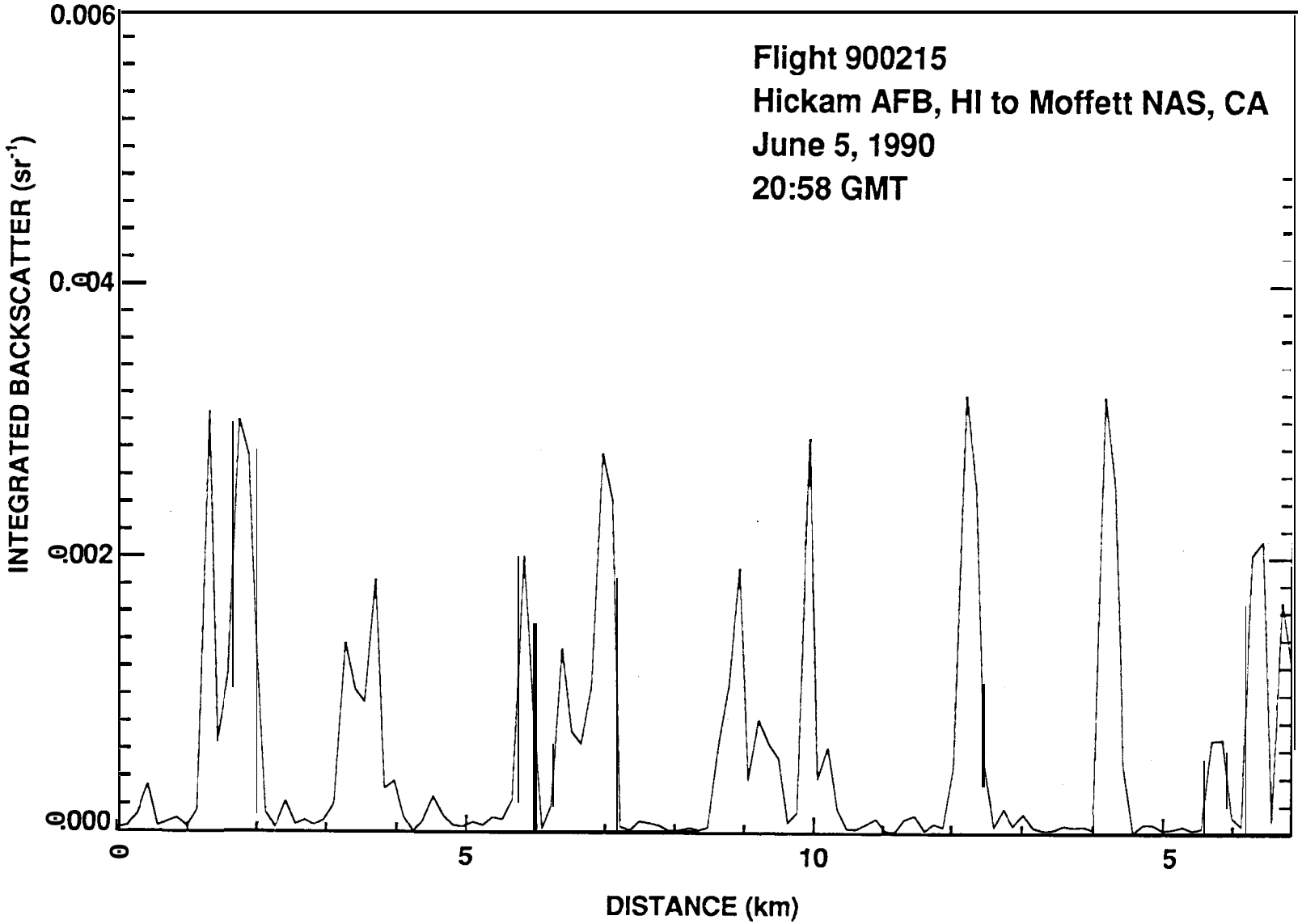
Flight 900215
Hickam AFB, HI to Moffett NAS, CA
June 5, 1990
20:58 GMT
INTEGRATED BACKSCATTER (sr-1)
0.006
0.004
0.002
0.000
0
5
10
5
DISTANCE (km)